

## SURFACE ALBEDO OBTAINED WITH MODIS IMAGES IN CASES OF LOW AND HIGH AEROSOL LOADING IN THE ATMOSPHERE

Juarez Dantas de Souza<sup>1</sup>, Juan Carlos Ceballos<sup>2</sup> and Bernardo Barbosa da Silva<sup>3</sup>

**ABSTRACT.** The surface albedo is a parameter of vital importance for estimating the net radiation. This parameter is obtained by using data obtained from satellite images and by utilizing the appropriate method for atmospheric correction. The method used by NASA (National Aeronautics and Space Administration) to obtain surface reflectance through MODIS (Moderate Resolution Imaging Spectrometer) sensor aboard the Terra and Aqua satellites (MOD09 and MYD09 products) has proved inaccurate for the detection of burning areas in the Amazon region – for products in both collection 4 and collection 5. Other methods have been used to obtain the albedo. However, these are limited to atmospheric conditions with negligible aerosol influence. In the present work, we have established a relationship between surface reflectance and the top of atmosphere, based on a radiative transfer model in an atmosphere of multiple layers. The method applied to products Level 1B (MOD02 and MYD02) in regions of low aerosol loading (Northeast Brazil) produces results similar to those effected by product MOD09. Furthermore, in regions of high aerosol loading (burnings in the Amazon region of Brazil), the method presents much higher performance than that rendered by the MOD09 and MYD09 products, improving, therefore, by more than 10% the accuracy of these results. The method is simple, efficient and easy to use.

**Keywords:** reflectance, atmospheric correction, method of two streams, burning regions.

**RESUMO.** O albedo da superfície é um parâmetro fundamental na estimativa do saldo de radiação. Ele pode ser obtido através de dados gerados por imagens de satélite, utilizando um método adequado de correção atmosférica. O método usado pela NASA (National Aeronautics and Space Administration), para obter refletâncias da superfície, através do sensor MODIS (Moderate Resolution Imaging Spectrometer) abordo dos satélites Terra e Aqua (produtos MOD09 e MYD09), apresenta problemas em regiões de queimadas na Amazônia, tanto os produtos da coleção 4 como os da coleção 5. Outros métodos têm sido utilizados para a obtenção do albedo. No entanto, eles são limitados à aplicação em atmosfera com pouca influência de aerossol. Neste trabalho, é estabelecida uma relação entre a refletância da superfície e a do topo da atmosfera, com base em um modelo de transferência radiativa numa atmosfera de múltiplas camadas. O método aplicado aos produtos nível 1B (MOD02 e MYD02), em regiões de baixa carga de aerossol (Nordeste do Brasil), produz resultados semelhantes ao produto MOD09, e em regiões de alta carga de aerossol (região de queimadas na Amazônia brasileira), apresenta desempenho superior aos produtos MOD09 e MYD09, melhorando em mais de 10% a precisão desses resultados. O método é simples, eficiente e de fácil utilização.

**Palavras-chave:** refletância, correção atmosférica, método de dois fluxos, região de queimadas.

---

<sup>1</sup>Department of Mathematics, Universidade Estadual da Paraíba, Centro de Ciências e Tecnologia – CCT, Rua Juvêncio Arruda, 351, Campus Universitário (Bodocongó), 58109-790 Campina Grande, PB, Brazil. Phone-Fax: +55(83) 3315-3340 – E-mail: juarezdantas@hotmail.com

<sup>2</sup>Division of Environmental Systems and Satellites, Center for Weather Forecasting and Climate Studies, Instituto Nacional de Pesquisas Espaciais, Rodovia Presidente Dutra km 40, 12630-000 Cachoeira Paulista, SP, Brazil. Phone: +55(12) 3186-9399; Fax: +55(12) 3186-9291 – E-mail: juanc\_cebillos@hotmail.com

<sup>3</sup>Academic Division of Atmospheric Sciences, Center for Technology and Natural Resources, Universidade Federal de Campina Grande, Av. Aprígio Veloso, 822, Bairro Universitário, 58429-120 Campina Grande, PB, Brazil. Phone: +55(81) 21016-1202 – E-mail: bbdasilva.ufpe@gmail.com

## INTRODUCTION

Several studies rate the surface albedo as a key parameter to assess energy balance at the Earth's surface. Given its importance, the search for practical and reliable methods of remote sensing, capable of providing consistent results, has been the central concern of all organs involved.

In order to estimate the surface reflectance taken from top atmosphere, one needs to eliminate the influence of the effects of both absorption and dispersion caused by atmospheric components. Accordingly, the use of the Radiative Transfer Equation (RTE) is most suitable for making an atmospheric correction. However, complexity, lack of knowledge and difficulties concerning the use of codes and radiative transfer models are some of the obstacles encountered by many users. As a result, users end up by adopting other methods (Liang et al., 2001; Song et al., 2001; Schroeder et al., 2006) that, despite their limitations, have become popular for their easiness of use. Some of these methods utilize only the information provided by the image itself; for example, a dark pixel. Because this type of pixel presents very low reflectance on the earth-atmosphere system, it is largely used to quantify the interference caused by atmospheric effects on the whole scene. These methods may be simple and unsophisticated, but they are certainly inaccurate. The DOS method (Dark Object Subtraction) developed by Chavez (1988) is surely the most popular and the most simple of all (Song et al., 2001). In order for the same to be applied, the image should contain water-covered surfaces, shadows due to topography and/or other features of low reflectance for which it is assumed that the reflectance is 1%. These methods do present a number of errors when evaluating the reflectance upon the infra-red (Moran et al., 1992). On the other hand, these methods fail to produce reliable results when the density of the vegetation area under investigation is not homogeneous (Liang et al., 2001). Such methods are not intended to correct atmospheric effects submitted to high aerosol loads (Song et al., 2001). The same occurs as well with other methods that employ empirical functions for estimating the reflectance and transmittance of the atmosphere. For that matter, these methods are limited by the variability of the atmospheric constituents. As usual, these methods may be practical, but their accuracy thereof depends on the similarity between the real atmospheric profile and the one taken as typical. Aerosols, for example, are highly variable in time and space; therefore, one should not oversimplify by stating that the entire atmosphere, even that resting over rural areas, has the same profile and the same amount of aerosol. Considering the circumstances, for example, those involving agricultural activities and the transportation of aerosol from one

region on to another, this can change the local atmospheric composition, endangering, as a result, the accuracy of empirical methods. Hence, the methods involving ETR are more reliable. Taking this into account, the 6S (Second Simulation of the Satellite Signal in the Solar Spectrum, Vermote et al., 1997) method is most recommended. With this method, atmospheric reflectance and transmittance are calculated by employing the method of successive orders of scattering. This method provides a good estimate of scattered radiation in the atmosphere. However, due to the inherent complexity of methods based on ETR, the search for simpler yet accurate methods has been intensified.

Twice a day, NASA makes available surface reflectance data derived from MODIS, duly corrected from all atmospheric effects, along seven spectral bands with a spatial resolution of 250 m (bands 1 and 2) and 500 m (bands 3, 4, 5, 6 and 7) by means of products such as: the MOD09 (product Terra satellite, which crosses over the Equator at 10:30 h) and the MYD09 (product Aqua satellite, which crosses over the Equator at 13:30 h). Albedo and reflectance products are also made available via a combination of two platforms (Terra/Aqua), among which the MCD43A3 product described in Table 1. In this work, one can see that the method used by NASA in regions with high aerosol load presents some major errors, involving products from both collection 4 and collection 5. On the other hand, by filtering the image quality during the period of 16 days, the albedo product MCD43, discard image data that have high aerosol load (Liu et al., 2009). Measurements with net radiometer, in a cultivated area, in northeastern Brazil local rural atmosphere with low aerosol load, show that the method presented by Tasumi et al. (2008) produces good results in obtaining the surface albedo. The surface reflected radiation is proportional to the intensity of the radiation falling on it. This is attenuated by various atmospheric components, mainly aerosol.

Then, in the composition of the resulting albedo of the seven MODIS bands, the subsequent weights concerning bands 3 and 4, spectral regions where the aerosol exerts a strong influence on the atmosphere, should not be fixed, since the setting of these weights may lead to errors in the calculation of the albedo in regions with a strong incidence of aerosol. The solution of the ETR in a real atmosphere is rather complex. A simpler solution may be obtained by using the 2-Flux Method (M2F) (Meador & Weaver, 1980). There would be no problems using this method on atmospheric correction, if the satellite calculated the irradiance, and if the atmosphere scattering were perfectly isotropic; however, this is not the case at all. Under such conditions, to use the M2F with the purpose of creating a relationship between surface reflectance ( $R_s$ ) and the radiance measured by satellite ( $L$ ), some adjust-

ments would be required in order to compensate for the effects of anisotropy and multiple scattering between the surface and atmosphere. Souza (2008) applied a solution of M2F in association with a stochastic model (Ceballos, 1989) in an atmosphere stratified into 16 homogeneous layers in order to establish a relationship between  $L$  and  $R_s$ , deduced from the equation of radiation balance at the top of the atmosphere (Vonder Haar & Kidder, 1995). For that, measurements at the surface at the time of the satellite overpass were used, simulations with aerosol loads between 0.05 and 1.2 and various types of surface (water, vegetation and bare soil) were simulated. Hence, an adjustment factor to the association between  $L$  and  $R_s$  was found.

The aim of this paper is to present a simple and efficient method to correct atmospheric effects on MODIS bands at the presence of aerosol and either high or low loads, obtaining, as a result, products from MODIS sensor radiance to surface reflectance on each band. Consequently, by using the method presented by Tasumi et al. (2008), one obtains the albedo of the whole solar spectrum.

**METHODOLOGY**

**Data**

The surface albedo was estimated by means of atmospheric correction on images of radiance, the MOD02 product (Earth platform radiance product) and MYD02 (Aqua radiance platform product). These products, with spatial resolution of 500 m, are available on: <<http://landsweb.nascom.nasa.gov/data/search.html>>, access on January 10<sup>th</sup>, 2010. It offers the radiance at the top of the atmosphere with information on the earth-atmosphere system. Through this radiance, the planetary reflectance ( $A_p$ ) is obtained, and correcting the atmospheric effects, the surface reflectance ( $R_s$ ) is also obtained. To correct atmospheric effects, the functions of transmittance and reflectance of the atmosphere were estimated with M2F. The M2F has as input: aerosol information, water vapor, solar zenith angle, surface pressure and ozone. Five sectors were selected from various regions of Brazil, as shown in Figure 1; namely: sector A1 (surface covered by the *Caatinga* with some irrigated areas, rural area of Ceará – CE); A2 (surface covered by the *Caatinga* of Paraíba – PB); A3 (surface covered by *Cerrado*, vegetation in the interior of São Paulo – SP); A4 (area covered by forest, Cuiabá – MT) and A5 (area covered by forest, Alta-floresta – MT). The sectors A1, A2 and A3 are located in rural areas where the load of aerosol in the atmosphere is less than 0.09; sectors A4 and A5 are those where the aerosol load varies from 0.21 to 1.37.

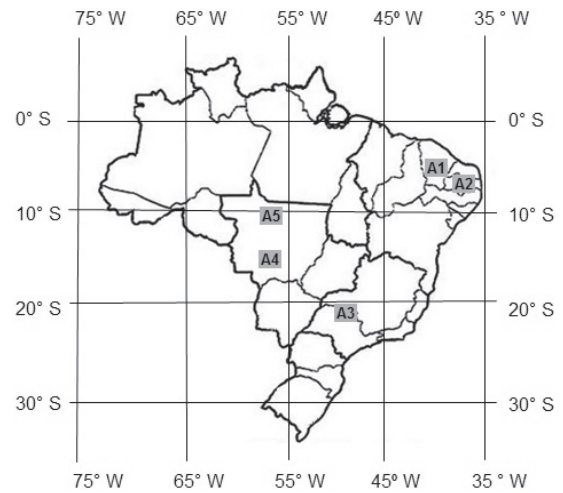


**Figure 1** – Sectors A1, A2, A3, A4 and A5, selected to implement atmospheric corrections by using the methods described in the present work.

Table 1 exhibits the data used in this study. They were derived from the MODIS sensor, and are described as follows: Earth platform (MOD02, MOD04, MOD07, MOD08, MOD09 and MOD43); Aqua platform (MYD02, MYD07, MYD08 and MYD09), platforms Terra/Aqua (combined product: MCD43A3); and data from the AERONET (AERosol Robotic NETwork) aerosol. In sectors A1, A2 and A3, for lack of information on the properties of aerosols, simple albedo ( $\omega$ ) and asymmetry ( $g$ ) factor, we used the method recommended by Shettle & Fenn (1979) and in sectors: A4 and A5, we used the AERONET data.

Table 2 shows the cases (10 in all) where the method presented in this work was compared to MCD43A3, MOD/MYD09 and Tasumi et al. (2008).

**Surface measurements**

In areas A1, A2 and A3, measurements were taken on the surface at intervals of 30 minutes. These were obtained by means of a net radiometer CNR1 (Campbell Scientific Net Radiometer), placed two meters above the surface in order to measure global radiation both incident and reflected with two inverted pyranometer models CM3 with accuracy  $\pm 2.5\%$  in the spectral range 0.3 to 2.8  $\mu\text{m}$ . In certain areas, the surfaces are not perfectly homogeneous. They show small variations regarding the intensity of vegetation, but they enable us to do comparisons from satellite data with higher spatial resolution (in our work, the data resolution was that of 500 m). In the A1 sector, the point of measurement (5°05'37"S, 37°50'22"W) is that of an irrigated banana plantation with a surface area of about 3 km<sup>2</sup>, located in the countryside of the State of Ceará. In A2 sector, the point of measurement (7°17'34"S, 36°29'08"W) is on *Caatinga*, with an area larger than 5 km<sup>2</sup>,

**Table 1** – Identification of MODIS products used for atmospheric correction applied to images of MODIS radiance.

Product	Description
MOD/MYD02 (*)	Product of radiance on 36 bands generated from MODIS sensor data. The radiance of bands 1-7 generates the reflectance of the earth-atmosphere system, influenced by the effects of scattering and absorption in the atmosphere. Available on: < <a href="http://ladsweb.nascom.nasa.gov/">http://ladsweb.nascom.nasa.gov/</a> > and < <a href="http://reverb.echo.nasa.gov/">reverb.echo.nasa.gov</a> >, accessed on June 6 <sup>th</sup> , 2012.
MOD09ghk	Provides the surface reflectance obtained from the product of radiation, adjusted for the effects of scattering and absorption in the atmosphere (collection 4), bands 1-7 (centered at 0.648 $\mu$ m, 0.858 $\mu$ m, 0.470 $\mu$ m, 0.555 $\mu$ m, 1.240 $\mu$ m, 1.640 $\mu$ m and 2.130 $\mu$ m, respectively). Note: This product is no longer available from NASA.
MOD/MYD09ga (*)	Surface reflectance product, collection 5, resulting from improvements in collection 4 (MOD/MYD09ghk). Available on: < <a href="http://reverb.echo.nasa.gov/">reverb.echo.nasa.gov</a> >, accessed on June 6 <sup>th</sup> , 2012.
MOD/MYD08 (*)	Product comprising data on aerosol clouds, precipitable water and atmospheric profile, spatial resolution of $1 \times 1^\circ$ . Available on: < <a href="http://ladsweb.nascom.nasa.gov/">http://ladsweb.nascom.nasa.gov/</a> >, accessed June 6 <sup>th</sup> , 2012.
MCD43A3 (*)	Product derived from a combination of the platforms Terra/Aqua, collection 5. With spatial resolution of 500 m, and 16 days temporal in cycles of 8, it provides directional hemispheric reflectance (black-sky albedo) and bidirectional (white-sky albedo). Available on: < <a href="http://ladsweb.nascom.nasa.gov/">http://ladsweb.nascom.nasa.gov/</a> >, accessed June 6 <sup>th</sup> , 2012.
MOD/MYD07 (*)	Product composed of several parameters, including solar zenith angle, surface pressure, precipitable water, ozone, aerosol load and Angström exponent with a resolution of 5 km. Available on: < <a href="http://ladsweb.nascom.nasa.gov/">http://ladsweb.nascom.nasa.gov/</a> >, accessed June 6 <sup>th</sup> , 2012.
MOD04 (*)	This product features: solar zenith angle, aerosol load and Angström exponent with a resolution of 10 km. Available on: < <a href="http://ladsweb.nascom.nasa.gov/">http://ladsweb.nascom.nasa.gov/</a> >, accessed on June 20 <sup>th</sup> , 2011.
AERONET	Aerosol RObotic NETwork. Available on: < <a href="http://aeronet.gsfc.nasa.gov/">http://aeronet.gsfc.nasa.gov/</a> >, access on June 20 <sup>th</sup> 2012, offers parameters aerosol: optical depth, albedo and simple asymmetry factor.

(\*) Source: NASA, MODIS website.

located in the countryside of the State of Paraíba. The point of measurement (21°37'24"S, 47°39'27"W) of the A3 sector lies over an area of *Cerrado*, spread over an area larger than 4 km<sup>2</sup>, located in the countryside of São Paulo. Comparisons were made based on measurements at satellite overpass times. In sectors: A4 and A5, no surface measurements were conducted. Thus, in the A4 sector, a series of images was selected (see Table 2) with information from surface reflectance, before, during and after burning periods. In this case, if in the earth-atmosphere system only the aerosol load was altered, an efficient method of atmospheric correction should eliminate effects caused by aerosol, and with acceptable accuracy to reproduce the same value of albedo before, during and after the period of burned. Whereas in the A5 sector, we selected an area containing black pixels (possibly a river) plus two other cases: a day with low aerosol load in the atmosphere

and another day with very high load. Thus, as in the previous case, an efficient method can eliminate the effects caused by aerosol albedo and reproduce the same albedo in both cases.

Reflectance products from MODIS are offered along seven spectral bands. Table 3 shows the width of each band and its extension. The bands were widened, as suggested by Tasumi et al. (2008) so as to equal the same spectral range of CNR1 (0.3 to 2.8 $\mu$ m). In this work the surface albedo ( $A_s$ ) represents the reflectance of such range.

### Method

The surface albedo is obtained by converting the seven spectral bands (Liang et al., 1999; Tasumi et al., 2008). In the present work, the conversion of spectral reflectance into albedo is obtained as recommended by Tasumi et al. (2008).

**Table 2** – Data on the sectors illustrated in Figure 1. In each case: MODIS reflectance product, data, precipitable water ( $w$ ), properties of the aerosol {optical thickness ( $\tau$ ) at  $0.55\mu\text{m}$ , Angström coefficient ( $\alpha$ ), simple albedo ( $\omega$ ) asymmetric factor, ( $g$ )} and data source (superscript in parenthesis).

Sector	Case	Reflectance Product	Date Day of the year	$\tau(0.55)$	$\alpha$	$\omega$	$g$	w(cm)	Zenith (°) Sun/Sensor
A1	1	MOD09ghk MCD43A3	10/12/2005 (344)	0.085 <sup>(1)</sup>	0.42 <sup>(1)</sup>	0.93 <sup>(2)</sup>	0.64 <sup>(2)</sup>	3.7 <sup>(3)</sup>	24.6/17.0
A2	2	MOD09ghk MCD43A3	12/07/2005 (193)	0.053 <sup>(1)</sup>	1.809 <sup>(1)</sup>	0.93 <sup>(2)</sup>	0.64 <sup>(2)</sup>	3.0 <sup>(3)</sup>	37.0/17.0
A3	3	MOD09ghk MCD43A3	16/07/2005 (197)	0.045 <sup>(1)</sup>	0.868 <sup>(1)</sup>	0.93 <sup>(2)</sup>	0.64 <sup>(2)</sup>	2.4 <sup>(3)</sup>	49.0/2.2
A4	4	MOD09ghk/ga MCD43A3	17/08/2005 (229)	0.21 <sup>(1)</sup>	0.624 <sup>(1)</sup>	0.91 <sup>(5)</sup>	0.62 <sup>(5)</sup>	3.0 <sup>(5)</sup>	37.2/22.4
	5	MOD09ghk/ga MCD43A3	26/08/2005 (238)	0.80 <sup>(1)</sup>	0.843 <sup>(1)</sup>	0.96 <sup>(5)</sup>	0.62 <sup>(5)</sup>	3.7 <sup>(5)</sup>	35.7/8.6
	6	MOD09ghk/ga MCD43A3	28/08/2005 (240)	1.07 <sup>(1)</sup>	1.400 <sup>(1)</sup>	0.93 <sup>(5)</sup>	0.62 <sup>(5)</sup>	2.9 <sup>(5)</sup>	35.2/19.8
	7	MOD09ghk/ga MCD43A3	04/09/2005 (247)	0.99 <sup>(1)</sup>	1.500 <sup>(1)</sup>	0.91 <sup>(5)</sup>	0.64 <sup>(5)</sup>	3.2 <sup>(5)</sup>	37.2/7.4
	8	MOD09ghk/ga MCD43A3	16/09/2005 (259)	0.45 <sup>(1)</sup>	1.654 <sup>(1)</sup>	0.80 <sup>(5)</sup>	0.58 <sup>(5)</sup>	3.6 <sup>(5)</sup>	26.0/38.0
A5	9	MOD09ga	16/08/2007 (228)	0.64 <sup>(4)</sup>	0.69 <sup>(4)</sup>	0.81 <sup>(5)</sup>	0.58 <sup>(5)</sup>	2.6 <sup>(5)</sup>	31.5/4.0
	10	MOD09ga	23/08/2007 (235)	1.37 <sup>(4)</sup>	1.43 <sup>(4)</sup>	0.88 <sup>(5)</sup>	0.59 <sup>(5)</sup>	3.5 <sup>(5)</sup>	31.9/10.0

Reference: <sup>(1)</sup>MOD08, <sup>(2)</sup>Shettle & Fenn (1979), <sup>(3)</sup>MOD07, <sup>(4)</sup>MOD04, <sup>(5)</sup>AERONET.

**Table 3** – Distribution along increasing escalation of solar spectrum, spectral bands of MODIS and extended bands, according to Tasumi et al. (2008).

Bands	Band width ( $\lambda_1, \lambda_2$ )( $\mu\text{m}$ )	Broad band ( $\lambda_1, \lambda_2$ )( $\mu\text{m}$ )
3	(0.460, 0.480)	(0.300, 0.515)
4	(0.545, 0.570)	(0.515, 0.595)
1	(0.620, 0.670)	(0.595, 0.755)
2	(0.840, 0.875)	(0.755, 1.055)
5	(1.230, 1.250)	(1.055, 1.440)
6	(1.630, 1.650)	(1.440, 1.830)
7	(2.105, 2.155)	(1.830, 2.800)

Defining  $R_A$ ,  $T_a$  and  $T_d$  as the reflectance, upward and downward transmittance, respectively, from the atmosphere, and considering multiple reflections between the surface and the atmosphere, the irradiance reflected by the Earth-atmosphere system ( $E_{AR}$ ) can be expressed as follows (Lenoble, 1985):

$$E_{AR} = E_0 [R_A + R_s T_a T_d / (1 - R_s R_A)] \quad (1)$$

where  $E_o = \mu_o S_o$ , and  $S_o$  is the spectral irradiance ( $\text{Wm}^{-2}\mu\text{m}^{-1}$ ) with direct solar incidence,  $\mu_o$  is the cosine of the solar zenith angle, and the expression  $1/(1 - R_s R_A)$  represents the contribution from multiple reflections between the atmosphere and the surface. According to Lenoble (1985), the total irradiance absorbed by the surface ( $E_g$ ) is:

$$E_g = E_o T_d (1 - R_s) / (1 - R_s R_A) \quad (2)$$

where  $E_o T_d$  represents the first-order irradiance to reach the surface. In Eqs. (1) and (2), taking  $E_o T_d = E_{sup}$  and  $k = 1/(1 - R_s R_A)$ , the equation of radiative balance (monochromatic) of the earth-atmosphere system, according to Kidder & Vonder Haar (1995), is:

$$E_o = E_{AA} + E_{sup}(1 - R_s)k + E_{AR} \quad (3)$$

where  $E_{AA}$  is the irradiance absorbed by the atmosphere. Considering the earth-atmosphere system as isotropic,  $E_{AR}$  represents the irradiance as measured by the satellite ( $\pi L$ ). Thus, by

resolving Eq. (3) to  $R_s$ , we have:

$$R_s = 1 - (E_o - E_{AA} - \pi L) / k E_{SUP}. \quad (4)$$

In this equation,  $E_{AA}$  and  $E_{sup}$  are intrinsic to the atmosphere; thus, the following is obtained for  $R_s = 0$ , that is to say in Eq. (3),  $k = 1$  and  $E_o - E_{AA} = E_{sup} + E_{AR}$ . Therefore, the direct relationship between  $R_s$  and  $\pi L$  can be established as:

$$R_s = a\pi L + b \quad (5a)$$

where:

$$a = 1/k E_{SUP} \quad (5b)$$

$$b = [(k - 1)E_{SUP} - E_{AR}] / k E_{SUP} \quad (5c)$$

and the role of  $k$  is to compensate for the effects of scattering anisotropy caused by molecules and aerosols, which decrease as wavelength increases with an increase of wavelength. For the MODIS sensor, wavelength along the 7 bands (1, 2, 3, ..., 7) increases in the order: 3, 4, 1, 2, 5, 6 and 7. These bands are affected by absorption due to water vapor; whereas, in bands 5, 6 and 7, scattering effects may be ignored. In Eqs. (5a), (5b) and (5c),  $L$ ,  $E_{SUP}$  and  $E_{AR}$ , vary with the sun zenith angle and the aerosol load. In all cases shown in Table 2, the aerosol load was kept constant throughout the experiment. So, after a number of simulations with Eq. (5a), an empirical expression was defined for  $k$ . In these simulations,  $\pi L$  is derived from the MODIS sensor. The albedo is measured on the surface, and the irradiances  $E_{SUP}$  and  $E_{AR}$  are assessed by means of the two-stream stochastic model M2F (Ceballos, 1989; Souza et al., 2008). In the M2F, the atmosphere was stratified into 16 layers. The atmosphere transmittance and reflectance on each band were integrated by means of a spectral resolution of  $0.005\mu\text{m}$ . According to Souza et al. (2008), M2F produces similar results to those of SBDART (Santa Barbara DISORT Atmospheric Radiative Transfer) (Ricchiazzi et al., 1998). Finally, we defined  $k$  as function of  $\tau(0.55)$  and  $\mu_o$  for each MODIS band  $i$ , as the expressions (Souza, 2008):

$$k_3 = 1.065 + 0.11\tau - 0.03\mu_o \quad (6a)$$

$$k_1 = k_3 - 10.05\eta \quad (6b)$$

$$k_2 = k_3 - 15.2\eta \quad (6c)$$

$$k_4 = k_3 - 5\eta \quad (6d)$$

$$k_5 = k_6 = k_7 = 1 \quad (6e)$$

$$\eta = (k_3 - 1) / 20.55 \quad (6f)$$

For example, in case 3 in Table 2 where  $\tau(0.55) = 0.045$ ;  $k_3 = 1.047$  (relatively small value), and case 6, where

$\tau(0.55) = 1.07$ ,  $k_3$  is less than 1.16. The  $k$  values decrease as the influence of the aerosol load on each MODIS bands, that is,  $k_3 > k_4 > k_1 > k_2 > k_5 = k_6 = k_7 = 1$ .

For the MODIS sensor band  $i$ , with width  $\Delta\lambda_i = \lambda_2 - \lambda_1$ , the reflectance ( $R_{s_i}$ ) was calculated according to the expressions (Souza, 2008):

$$R_{s_i} = a_i\pi L_i + b_i \quad (7a)$$

$$L_i = \Delta\lambda_i \cdot nd_i \cdot cal_i \quad (7b)$$

where  $nd_i$  is signal as registered by the satellite, and  $cal_i$  is the calibration constant (value attributed to the product of radiance).

The  $A_s$  on the spectral interval ranges from  $0.3$  to  $2.8\mu\text{m}$ , and is determined by the irradiance  $\{E_{SUP}(\lambda)\}$  and the reflected  $\{E_R(\lambda)\}$  on the surface according to the equation:

$$A_s = \frac{\int_{0.3}^{2.8} E_R(\lambda) d\lambda}{\int_{0.3}^{2.8} E_{SUP}(\lambda) d\lambda} \quad (8)$$

To convert the reflectance of the seven spectral bands of MODIS in  $A_s$ , the weight of each band ( $p_i$ ) is assessed by equation (Tasumi et al., 2008):

$$p_i = \frac{\int_{\lambda_1}^{\lambda_2} E_{SUP}(\lambda) d\lambda}{\int_{0.3}^{2.8} E_{SUP}(\lambda) d\lambda} \quad \sum_{i=1}^7 p_i = 1 \quad (9)$$

In these equations,  $\lambda_1$  and  $\lambda_2$  are the limits of the enlarged band as shown in Table 2. The fraction numerator represents the flow that reaches the surface on band  $i$ , and the denominator is the total flow band. Thus, this is estimated by the equation:

$$A_s = \sum_{i=1}^7 p_i R_{s_i} \quad (10)$$

To obtain  $A_s$  derived from the MCD43A3, the following expression was used (Schaaf et al., 2002):

$$A_s(\theta, \tau) = Rd(\theta, \tau)\alpha_{ws}(\theta, \tau) + \{1 - Rd(\theta, \tau)\}\alpha_{bsa}(\theta, \tau) \quad (11)$$

where  $Rd(\theta, \tau)$  represents the diffuse radiation fraction as a function of both the sun zenith angle ( $\theta$ ) and the aerosol optical depth ( $\tau$ );  $\alpha_{ws}(\theta, \tau)$  is the white-sky albedo (relative to the diffuse flow) and  $\alpha_{bsa}(\theta, \tau)$  is the black-sky albedo (relative to the flow direction). In Eq. (11),  $Rd(\theta, \tau)$  was estimated by the M2F.

## RESULTS AND DISCUSSION

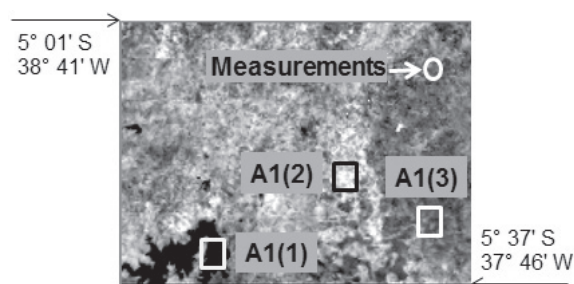
To facilitate the presentation of results, we define:  $A_s$ -M2F, the albedo estimated by the method presented in this work;  $A_s$ -Tasumi, the albedo estimated according to Tasumi et al. (2008);  $A_s$ -MOD09 as the albedo obtained from products of the earth platform;  $A_s$ -MYD09, the albedo obtained with the MYD09 products from the Aqua platform;  $A_s$ -MCD43, albedo of 16 days (combination Terra/Aqua); and  $A_s$ -Med, the surface albedo measured. In each section, data relating to aerosols are the same in all scenarios. In sectors: A1, A2 and A3, the collection 4 MODIS products were used, and for the sectors A4 and A5, products from collections 4 and 5 were used, these were called MOD09-C4 and MOD09-C5, respectively.

Table 4 shows the coefficients  $a$ ,  $b$ ,  $p$ , obtained from Eqs. (5) and (9), for the cases: 4 (lower aerosol load) and 6 (higher aerosol load), as described in Table 2. In both cases, the surface coverage is the same, and both the solar zenith angle and the amount of rain water in the atmospheric column are practically the same. Both cases exhibit similarities between the results obtained with the models M2F and SBDART. The biggest difference of about 20% occurs in the value of  $a$  on band 7; however, as the weight of the albedo composition is less than 4%, this difference is negligible.

At the top of the atmosphere, surface information is affected by scattering due to an increase of the aerosol load growth (Song et al., 2001). According to Souza et al. (2008), the increasing load of aerosol in the atmosphere reduces the irradiance intensity on the surface; on the other hand, scattering increases (Wang et al., 2010). As  $p$  [defined by Eq. (9)] represents the ratio between band irradiance and spectrum irradiance from 0.3 to  $2.8\mu\text{m}$ , an increasing aerosol load causes a reduction on bands 3, 4, 1 and 2 (where aerosols exert a strong influence) and an increase in bands 5, 6 and 7 (where aerosols influence is negligible). For clean rural atmosphere it would be acceptable to fix these weights, as suggested by Tasumi et al. (2008); however, in places where there are large aerosol variations, errors may occur in the calculation of albedo. Since the value of  $k$ , used in Eq. (4) and defined by Eqs. (6) is proportional to the aerosol increases in bands 3, 4, 1 and 2; and it is neutral ( $k = 1$ ) on bands 5, 6 and 7. With increasing aerosol loads, there occurs an increase in the scattering within the atmosphere, which augments the intensity of multiple scattering between the surface and the atmosphere, raising, as a result, the production of diffuse radiation on the surface, which affects the relationship between the reflectance on this surface and the reflectance at the top of the atmosphere [Eq. (5a)]. In this case, the value of  $k$  tunes up this relationship by offsetting the effects of these scatterings.

### Atmospheric correction: case 1 (A1 sector)

In this case, to make comparisons between methods: M2F, MOD09 (collection 4), Tasumi and MCD43, small areas were selected: A1(1) (covered by water, size:  $7 \times 13$  pixels, centered on:  $5^\circ 33'21''\text{S}$ ,  $38^\circ 26'53''\text{W}$ ); A1(2) (surface with apparent low vegetation density, size:  $12 \times 13$  pixels, centered on:  $5^\circ 22'31''\text{S}$ ,  $38^\circ 07'12''\text{W}$ ) and A1(3) (apparently with good surface density vegetation, size:  $12 \times 13$  pixels, centered on:  $5^\circ 24'09''\text{S}$ ,  $35^\circ 55'15''\text{W}$ ); and a point with surface measurements, described in previous section, as illustrated in Figure 2. The results obtained from earth satellite data were compared to measurements taken on the surface on December 10<sup>th</sup>, 2005, on the 344<sup>th</sup> day of the year, at 13:00 UTC (satellite overpassing time).



**Figure 2** – Sector A1,  $A_s$ -MOD09 image on day 344 of the year 2005, illustrations of areas A1(1), A1(2), A1(3) and site of measurements.

In Table 5, for each area and measurement places, we present results concerning the average albedo:  $A_s$ -M2F,  $A_s$ -Tasumi,  $A_s$ -MOD09,  $A_s$ -MCD43 and  $A_s$ -Med. The value in parenthesis is the standard deviation.

Deviations from the  $A_s$ -Med are:  $-0.001$  ( $A_s$ -M2F),  $+0.002$  ( $A_s$ -MOD09),  $-0.007$  ( $A_s$ -Tasumi) and  $-0.002$  ( $A_s$ -MCD43). In the area A1(1), the  $A_s$ -MCD43, compared to other methods, presented the differences:  $-0.021$  ( $A_s$ -M2F),  $-0.027$  ( $A_s$ -Tasumi) and  $-0.021$  ( $A_s$ -MOD09), which are relatively significant; however, due to lack of information concerning other results and site measurements, it is not possible to draw in further considerations. In areas A1(2) and A1(3), the three methods give very similar results. The difference between the  $A_s$ -MCD43 and the other is less than 0.008. These differences, together with the standard deviation show that the methods in these areas exhibit similar values.

In Figures 3a, 3b and 3c, one observes the behavior of the average albedo on each column of the pixel matrix on the areas A1(x). Figures 3d, 3e and 3f illustrate the behavior of reflectance on the seven bands of MODIS.

In the area A1(1), Figure 3a, the three methods:  $A_s$ -M2F,  $A_s$ -MOD09 and  $A_s$ -Tasumi have almost the same behavior,

**Table 4** – Coefficients  $a$ ,  $b$ , and  $p$  obtained from the M2F and SBDART on days 229 [ $\tau(0.55) = 0.21$ ; precipitable water = 2.9 cm] and 240 [ $\tau(0.55) = 1.07$ ; precipitable water = 2.4 cm].

Day	Model	Coef.	Bands						
			3	4	1	2	5	6	7
229	SBDART	$a$	0.038	0.032	0.018	0.041	0.150	0.299	0.348
		$b$	-0.098	-0.044	-0.032	-0.023	-0.025	-0.020	-0.015
		$p$	0.249	0.126	0.209	0.225	0.097	0.063	0.031
	M2F	$a$	0.037	0.032	0.018	0.040	0.154	0.303	0.285
		$b$	-0.094	-0.044	-0.033	-0.022	-0.025	-0.018	-0.017
		$p$	0.245	0.130	0.216	0.223	0.087	0.062	0.037
$k$			1.064	1.049	1.033	1.017	1.000	1.000	1.000
240	SBDART	$a$	0.047	0.037	0.020	0.037	0.152	0.297	0.340
		$b$	-0.229	-0.128	-0.103	-0.072	-0.059	-0.037	-0.023
		$p$	0.206	0.119	0.210	0.243	0.111	0.074	0.037
	M2F	$a$	0.045	0.036	0.020	0.043	0.160	0.305	0.279
		$b$	-0.226	-0.135	-0.114	-0.079	-0.070	-0.043	-0.030
		$p$	0.204	0.122	0.216	0.241	0.100	0.072	0.045
$k$			1.159	1.120	1.081	1.041	1.000	1.000	1.000

**Table 5** – Results obtained from the mean albedo of the A1 sector on areas A1(1), A1(2), A1(3) and albedo from the measurements area on day 344 in 2005, illustrated in Figure 2.

Place	$A_p$	$A_s$ -M2F	$A_s$ -Tasumi	$A_s$ -MOD09	$A_s$ -MCD43	$A_s$ -Med
Measurements	0.171	0.154	0.157	0.148	0.153	0.155
A1(1)	0.089(0.008)	0.067(0.009)	0.070(0.009)	0.069(0.013)	0.043(0.011)	X
A1(2)	0.227(0.018)	0.213(0.019)	0.219(0.020)	0.213(0.023)	0.221(0.018)	X
A1(3)	0.154(0.007)	0.137(0.007)	0.139(0.007)	0.136(0.012)	0.143(0.009)	X

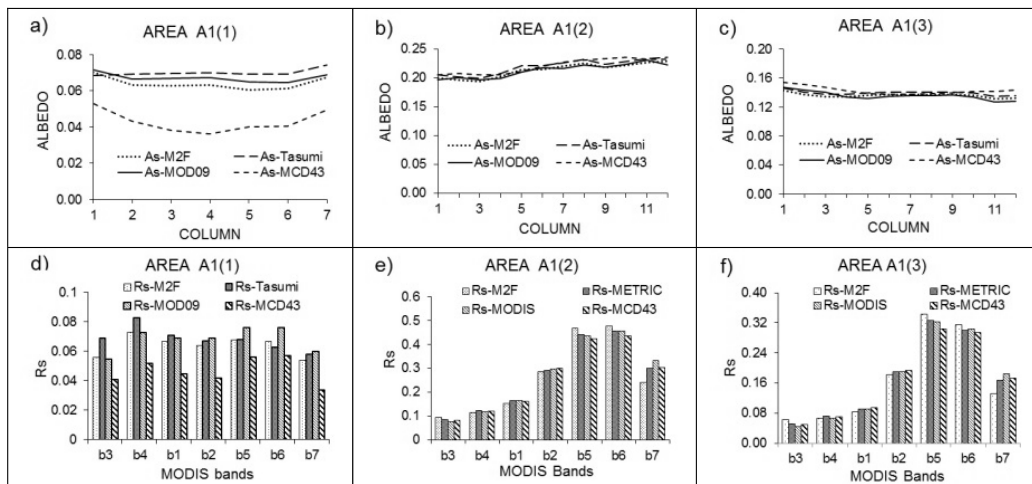


**Figure 3** – Results of surface albedo and reflectance on the MODIS seven bands on the site of measurements, and areas shown in Figure 2, obtained with the methods: M2F, Tasumi, MOD09 and MCD43; a, b and c are the result of the albedo on areas A(x), d, e and f. These are the results of reflectance on the seven bands of MODIS.



while the  $A_s$ -MCD43 differs somewhat from them. Regarding the reflectance, Figure 3d, shows that the  $R_s$ -M2F strikes a balance between the  $R_s$ -Tasumi and the  $R_s$ -MOD09. On bands 3, 4 and 1, where the  $R_s$ -Tasumi is the largest of all, the  $R_s$ -M2F is close to  $R_s$ -MOD09. On bands: 2, 5, 6 and 7, where the  $R_s$ -MOD09 is larger than the others, the  $R_s$ -M2F is close to  $R_s$ -Tasumi. In the case of the  $R_s$ -MCD43, though always less on all bands, it presents a rather consistent behavior in harmony with the others. On average, the relative deviations to  $R_s$ -MCD43 on seven bands are: +0.017 ( $R_s$ -M2F), +0.022 ( $R_s$ -Tasumi) and +0.021 ( $R_s$ -MOD09).

In the area A1(3), Figure 3c, with respect to  $A_s$ -MCD43, the average deviations: -0.007 ( $A_s$ -M2F), -0.004 ( $A_s$ -Tasumi) and -0.006 ( $A_s$ -MOD09) are similar to those in the area A1(2). Concerning Figure 3f, the three methods reproduce the same correlation between the spectral reflectance observed in the area A1(2). As to the spectral reflectance on the seven bands, Figures 3d, 3e and 3f, the average deviation of each method in relation to  $R_s$ -MCD43 is: 0.022 ( $R_s$ -M2F), 0.012 ( $R_s$ -Tasumi) and 0.014 ( $R_s$ -MOD09). These deviations are in agreement with the literature (Liang et al., 2002; Liu et al., 2009; Roman et al., 2011).

According to Table 2 (case 1), the aerosol load in the atmosphere is low  $\{\tau(0,55) = 0.085\}$ , and it exerts little influence on surface information recorded by the satellite sensor. Here, the values of  $k$ , defined by Eqs. (6) are relatively low (close to 1, i.e., neutral) on bands: 3 (1.044), 4 (1.033), 1 (1.022) and 2 (1.011). Under the conditions of case 1 (vegetated surface with aerosol load less than 0.3 and the solar zenith angle less than  $45^\circ$ ) the MOD09 compared to the MCD43 presents excellent results (Wang et al., 2010). Tasumi et al. (2008) estimated the surface albedo in vegetated areas accurately between -0.033 and +0.035, i.e. these represent far more serious mistakes than those found in the present section. In general, the differences between the methods in areas A1(1), A1(2), A1(3) and the measuring points are in accordance with Liang et al. (2002). The errors verified on the MODIS bands may be associated to lack of precision concerning the aerosol and water vapor data (Liang et al., 2002). The aerosol load used on the M2F is the same as that used on the MODIS; however, the simple albedo and the asymmetry factor are different. MODIS uses its own model (Wang et al., 2010), and the M2F uses Shettle & Fenn's model (1979). According to Vermote et al. (2002), MODIS has problems on band 3 due to uncertainties with aerosols; therefore, errors on this band may vary between 7% and 13%. According to Wang et al. (2010), there are many results where MODIS underestimates the reflectance on the visible. In this section, the results have shown that the absolute difference between the M2F and the MCD43 on bands 5 and 6 is approximately

+0.03, and 0.04 on band 7. The errors on the band 7 are of minor importance because this band used only 4% of the total incident solar energy at the top of the atmosphere, and on the albedo, it causes error of approximately 0.001 (Tasumi et al., 2008).

### Atmospheric correction: case 2 (A2 sector)

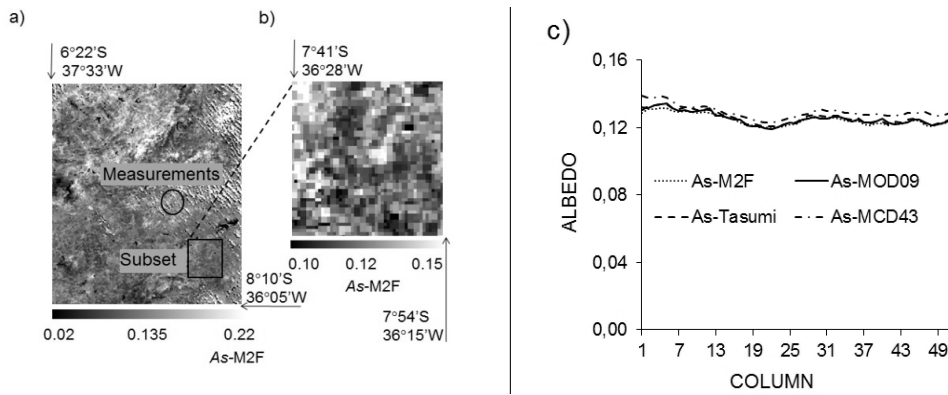
The A2 sector is a *Caatinga* area, on which the surface at measurement time (rainy period) showed good vegetation density. The site of measurement was an area of over 4 km<sup>2</sup> and considered homogeneous, making it possible to draw comparisons with satellite data. Measurements were made at the Earth satellite overpassing time on July 12<sup>th</sup>, 2005, on the 193<sup>rd</sup> day of the year, at 12:55 UTC.

Figure 4a represents the  $A_s$ -M2F on the A2 sector. It illustrates the location of measurements ( $7^\circ 17' 29''$ S;  $36^\circ 29' 04''$ W) on a patch of  $51 \times 51$  pixels of 500 m. Figure 4b depicts the  $A_s$ -M2F subset and Figure 4c illustrates the average albedo on each column of the subset's pixel matrix.

In Table 6, the results correspond to the average albedo from the A2 sector subset and to the albedo on the measurement site. It is observed that the results from  $A_s$ -MOD09,  $A_s$ -M2F,  $A_s$ -Tasumi and  $A_s$ -MCD43 are very close to those found in  $A_s$ -MED. The difference between the estimated values found by the four methods and those obtained by the  $A_s$ -MED was found to be less than 0.012. In the subset mean albedo, the  $A_s$ -M2F and the  $A_s$ -MOD09 produced equal results. The methods, among themselves, do present difference smaller than 0.004 and the standard deviation nearly equals 0.008. In Figure 4c, the average albedo curves along the 51 columns of the subset have the same behavior; however, the  $A_s$ -MCD43 was found to be always superior to the others. On average, the difference found in the  $A_s$ -MCD43 in relation to the other methods is: 0.004 ( $A_s$ -M2F), 0.004 ( $A_s$ -MOD09) and 0.003 ( $A_s$ -Tasumi). These results, as observed in the literature (Liang et al., 2002; Liu et al., 2009; Wang et al., 2010), are excellent, and rather consistent with the results obtained in this work. In this case, the atmospheric data (aerosol load and precipitable water), solar zenith and view angle are very close to the data found in case 1, which are situations where the MODIS exhibits good accuracy (Wang et al., 2010). Therefore, considering the precision parameters emphasized in the previous section, there is a good consistency between the results obtained with those derived from M2F and MODIS products.

### Atmospheric correction: case 3 (A3 sector)

In this case, the satellite (Aqua) overpass happened on July 16<sup>th</sup>, 2005 (on the 197<sup>th</sup> day of the year) at 16:55 UTC. Figure 5a shows the  $A_s$ -MCD43 from the sector, illustrates a target with water



**Figure 4** – a) Scene of  $A_s$ -M2F on day 193 of the year 2005, in sector A2 indicating the site of measurements and subset with  $51 \times 51$  pixels; b) Scene of  $A_s$ -M2F in the subset area; c) average behavior of the surface albedo along the 51 columns of the subset area.

**Table 6** – Results obtained from the mean albedo of subset in sector A2 and the local albedo measurements on day 193 of the year 2005, illustrated in Figure 4.

	$A_s$ -M2F	$A_s$ -Tasumi	$A_s$ -MOD09	$A_s$ -MCD43	$A_s$ -Med
As on the target	0.138	0.140	0.139	0.140	0.148
As on the subset	0.125(0.008)	0.126(0.009)	0.125(0.008)	0.129(0.008)	X

coverage (P1), the location of surface measurements (P2) and a rectangular subset (size:  $278 \times 277$  pixels). In Figure 5b, the standard deviation (SD) is shown, the mode (most frequent value) and mean:  $A_s$ -M2F,  $A_s$ -Tasumi,  $A_s$ -MYD09 and  $A_s$ -MCD43, in relation to the subset. Finally, in Table 7 one can find the results for targets P1 and P2.

**Table 7** – Results obtained from application on the A3 area on day 197 of the year 2005. Entire area average albedo on target P2 (site with surface measurement) and on target P1 (surface covered by water).

	$A_s$ -M2F	$A_s$ -Tasumi	$A_s$ -MYD09	$A_s$ -MCD43	$A_s$ -Med
P1	0.017	0.008	0.019	0.014	X
P2	0.122	0.115	0.118	0.127	0.119

On P1 target, deviations from other methods with respect to  $A_s$ -MCD43 are: +0.003 ( $A_s$ -M2F), -0.006 ( $A_s$ -Tasumi) and +0.005 ( $A_s$ -MYD09), and on P2 target with respect to  $A_s$ -Med: +0.003 ( $A_s$ -M2F) -0.004 ( $A_s$ -Tasumi) -0.001 ( $A_s$ -MYD09) and +0.008 ( $A_s$ -MCD43).

In Figure 5b one finds the values for  $A_s$ -M2F,  $A_s$ -MYD09 and  $A_s$ -Tasumi. Their deviations in relation to the  $A_s$ -MCD43 are: a) the average: -0.004, 0.000 and -0.008; b) on the mode: -0.006, -0.000 and -0.006, and c) the standard deviation (SD): -0.001, 0.000 and 0.000. The results of this section are consistent with results of previous sections, and they have the same level of accuracy. In them, the  $A_s$ -Tasumi is always smaller than the other ones; however, the differences in relation to the MCD43 are in accordance with the authors (Tasumi et al., 2008).

Between the  $A_s$ -MYD09 and the  $A_s$ -M2F, the difference relative to the average (3%) and the mode (4.7%), according to the literature (Liang et al., 2002; Schroeder et al., 2006) can be considered optimal.

Considering the measurements on the surface, the results are good. However, small uncertainties have been noticed. It is very difficult to compare satellite data with surface measurements at a single point, especially when the surfaces are not perfectly homogeneous; increasing, as a result, uncertainties regarding satellite measurements (Román et al., 2011). In this case, comparisons could be more accurate if measurements were taken at several points and distributed according to the spatial resolution of the satellite. Even so, the measurements are still a reference used to verify the performance of these methods.

In the MCD43, the use of a BRDF (Bidirectional Reflectance Distribution Function) and the filtering of the data observed over the period of 16 days contributed to the differences with respect to the other methods which use daily data, because during the period of 16 days there may occur changes in the atmospheric composition (variations of aerosol and water vapor) and geometric variations (solar zenith and viewing).

In sectors: A1, A2 and A3, weather conditions are typical of rural atmosphere with low aerosol load. Under these conditions, MODIS produces excellent results (Wang et al., 2010). The method used in the MODIS product is a complex form of multiple scattering effects, and it works out correction effects from neighboring targets, indeed it can contribute to the differences observed

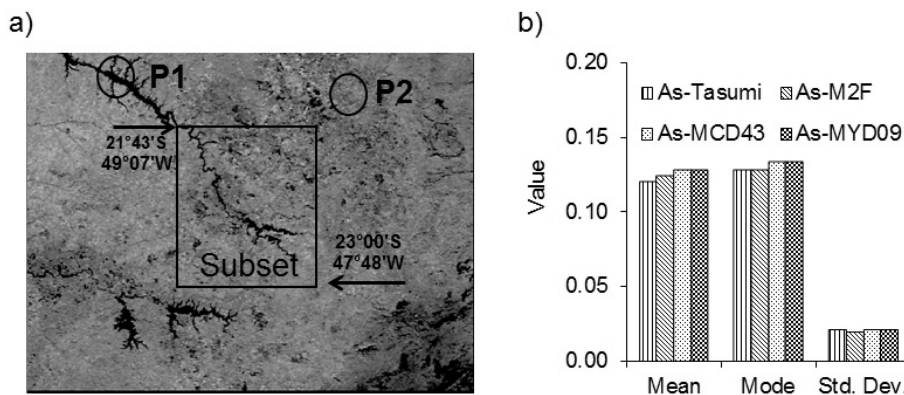


**Figure 5** – a) Scene of *As*-MCD43 on day 197 of the year 2005 in sector A3 with indication point on surface covered with water (P1), another on measurement areas (P2) and a subset of  $278 \times 277$  pixels. b) Subset albedo statistical data: standard deviation (SD), Mode and Mean.

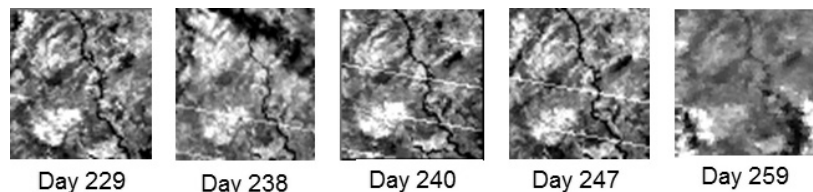
between MODIS and methods: M2F and Tasumi, since these do not correcting the effects of neighboring targets. Moreover, this correction presents several uncertainties, as Liang et al. (2001).

**Atmospheric correction: cases 4, 5, 6, 7, and 8 (A4 sector)**

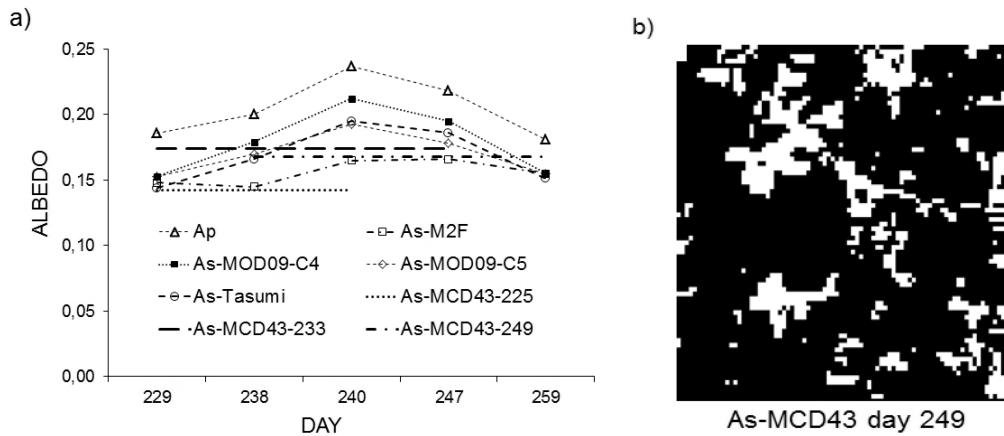
In cases 1, 2 and 3, based on the results presented in previous sections, atmosphere with low aerosol load, it was verified that the *As*-M2F and the *As*-Tasumi reproduce results with prime results approximation in relation to the albedo derived from MODIS product. In this section, we selected an area of  $73 \times 70$  pixels, in which there is a large aerosol variation in atmosphere: cases 4, 5, 6, 7, and 8 (Table 2) portray a burning period between 229 days (prior) and 259 days (later) in the Mato Grosso (MT) region. The results of *As*-M2F are compared to *As*-MOD09 (products from collections 4 and 5), *As*-Tasumi and *As*-MCD43. Figure 6 shows up scenes from *As*-M2F for days: 229, 238, 240, 247 and 259 in 2005. In Figure 7a, we present average values of *As*-M2F, *As*-MOD09-C4/C5, *As*-Tasumi, *As*-MCD43 and *A<sub>p</sub>* (planetary albedo) on days: 229, 238, 240, 247 and 259. Table 8, presents a summary of these results. The *As*-MCD43 was obtained from images displayed on days: 225, 233 and 249. According to Liu et al. (2009), the *As*-MCD43 may represent the surface albedo for 16 days either before or after processing. In this case, as shown in

Figure 7a, the albedo of day 225 may be the same for days: 229, 233 and 240; day 233 to day 229, 238, 240 and 247, and for day 249 for the days: 238, 240, 247 and 259.

In Figure 7a, it is noted that the *A<sub>p</sub>* is sensitive to radiation scattering caused by the aerosol in the atmosphere, increasing as it rises. The *As*-Tasumi and the *As*-MOD09 as well have exhibited the same effect. It was expected that the *As*-Tasumi was effective only in situations of atmosphere with low aerosol load, because this is an empirical method and, consequently, does not take into account the aerosol load in the atmosphere. It is designed only for clear sky with low aerosol loading. This method is not recommended to work out atmospheric corrections in the presence of high aerosol loads (Tasumi et al., 2008). By using a complex method of atmospheric correction, involving successive scattering commands, one would expect it to offer better results from the *As*-MOD09; however, this has not happened. However, it is worth noting that the product collection 5 (MOD09ga) performs better than that of collection 4 (MOD09ghk). The *As*-MCD43 (product of 16 days, with cycles of 8 days and resolution of 500 m) presents results based on the best geometric conditions (variations of zenith angles) and atmospheric (discarding situations with high aerosol loads or cloud cover) observed during the period. By discarding data with high aerosol loads, that is, by not correcting the atmospheric effects caused



**Figure 6** – Images of *As*-M2F in sector A4 on days: 229, 238, 240, 247 and 259 of the year 2005.



**Figure 7** – Results of average surface and planetary albedo ( $A_p$ ) in sectors A4: a) results of  $A_p$ ,  $A_s$ -M2F,  $A_s$ -Tasumi,  $A_s$ -MOD09 on days 229, 238, 240, 259, 247 of the year 2005, and b) the MCD43 scene on day 249 on which there is only information on the white-colored albedo.

**Table 8** – Surface and planetary albedo ( $A_p$ ) in sector 4 on days: 229, 238, 240, 247 and 259 of year 2005.

	229	238	240	247	259	Mean	Standard D.
$A_p$	0.186	0.200	0.237	0.218	0.181	0.204	0.021
$A_s$ -M2F	0.148	0.145	0.165	0.166	0.155	0.156	0.009
$A_s$ -MOD09-C4	0.153	0.179	0.212	0.195	0.155	0.179	0.023
$A_s$ -MOD09-C5	0.153	0.170	0.193	0.178	0.155	0.170	0.015
$A_s$ -Tasumi	0.144	0.166	0.195	0.186	0.151	0.168	0.020
$A_s$ -MCD43-225	0.142	0.142	0.142	–	–	–	–
$A_s$ -MCD43-233	0.174	0.174	0.174	0.174	–	–	–
$A_s$ -MCD43-249	–	0.168	0.168	0.168	0.168	–	–

by high aerosol loads, the images of MCD43 do not impart information of surface under these atmospheric conditions; for example, the image of the  $A_s$ -MCD43 of day 249 as illustrated in Figure 7b, has information only in the white color, equivalent to less than 50% of surface albedo information. Comparing the average albedo of days 229 and 259 (with low aerosol load) with the average albedo of the days 240 and 247 (with high aerosol load), the relative errors are: +9% ( $A_s$ -M2F), +32% ( $A_s$ -MOD09-C4), +20% ( $A_s$ -MOD09-C5) and +29% ( $A_s$ -Tasumi). Table 8 shows that on day 240 the surface the albedos in  $A_s$ -MOD09-C4/C5 and  $A_s$ -Tasumi are larger than the planetary albedo on days 229 and 259. This shows that these methods fail to correct effects due to high aerosol loads. In turn, the MCD43 shows different results for the same day. Comparing their results with that of M2F on days 229 and 238, the best approximation was that of  $A_s$ -MCD43-225; on days 240 and 247, the  $A_s$ -MCD43-249 is similar to that of  $A_s$ -M2F. On the other hand, the  $A_s$ -MCD43-233 overestimates the other ( $A_s$ -MCD43-225 and  $A_s$ -MCD43-249); however, on days 240 and 247, the difference in relation to  $A_s$ -M2F is negligible, i.e. less

than 0.009. Good accuracy requires an estimate error of 0.02 (Liang et al., 2002; Schroeder et al., 2006), thus, considering the standard deviation and the mean value of  $A_s$ -M2F, it would be acceptable to say that the  $A_s$ -MCD43-249 and the  $A_s$ -M2F have similar results. Disregarding the fact that the MCD43 results are only for favorable only to atmospheric correction situations, the M2F, on the other hand, covers all situations. These results show, according to Wang et al. (2010), that the MCD43 product provides results far more accurate than those offered by MOD09 products.

The purpose of atmospheric correction is to reduce the error when estimating surface reflectance (Song et al., 2001). Such errors, which can be caused by aerosols, do affect the accuracy of the corrected reflectance (Vermote et al., 2002). Errors in the MODIS reflectance bands increase as spray load increases (Wang et al., 2010.). For example, the aerosol load, which may concentrated on the troposphere, may result from a number of errors on units of reflectance (Vermote & Vermeulen, 1999). The accuracy of results, shown in Table 8, is in tune with the literature (Liang et al., 2002; Schroeder et al., 2006).

In Figure 8a, we present the average values of  $A_p$  and  $A_s$ -M2F, and in Figure 8b, the  $A_p$  and  $A_s$ -MOD09-C5 on days: 229, 240, 247 and 259, concerning the columns of pixels of the area shown in Figure 6. It is shown in these figures that the  $A_p$  on all columns has virtually the same behavior; but it significantly increases as the load aerosol increases. In Figure 8a, the  $A_s$ -M2F behavior is similar to that of the  $A_p$ , but it reproduces the surface albedo with good accuracy, i.e. the aerosol load varies from 0.021 to 1.07 which causes a variation that is less than 0.019 on the  $A_s$ -M2F. In Figure 8b, the  $A_s$ -MOD09-C5 presents also the same behavior, but it does not reproduce the gray surface albedo with good accuracy. We can see that  $A_s$ -MOD09-C5 on day 240 exceeds the  $A_p$  on days 229 and 259; in the same way that on day 247 it exceeds the  $A_p$  of day 259 between columns 15 and 22.

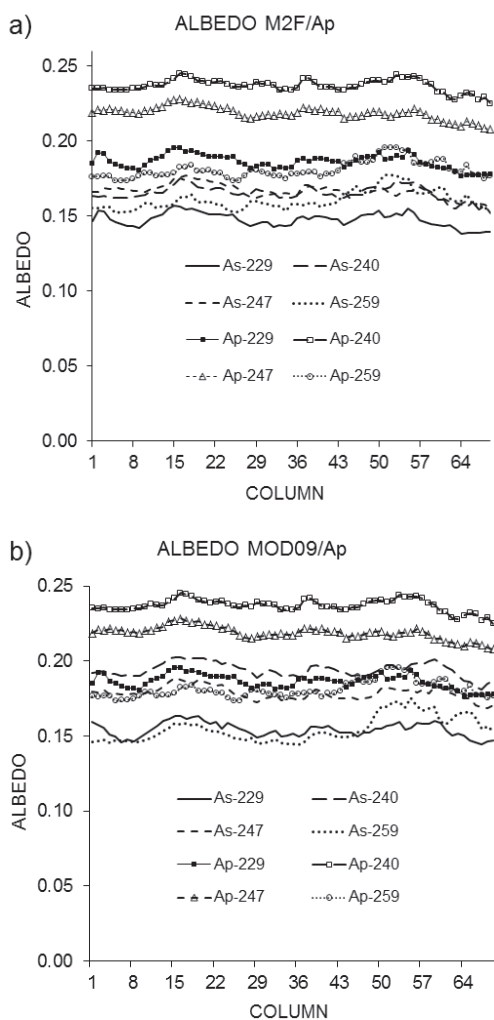


**Figure 8** – Average surface planetary albedo ( $A_p$ ) on days: 229, 240, 247 and 259 of the year 2005 on the 70 columns of the area shown in Figure 6. a) behavior of the  $A_p$  and the  $A_s$ -M2F; b) behavior of  $A_p$  and  $A_s$ -MOD09.

Figures 9a and 9b shows the results of spectral reflectance on the seven bands of MODIS on days 229 and 240. In Figure 9a, we compare the reflectance  $R_s$ -M2F with  $R_s$ -MOD09-C4, and in Figure 9b we compare the reflectance  $R_s$ -M2F with  $R_s$ -MOD09-C5. In these figures, it is noted that the  $R_s$ -M2F presents virtually the same behavior for days 229 and 240, especially on bands 3, 4, 1 and 2, a region where scattering by air molecules and aerosols is more intense. Yet, in the case of  $R_s$ -MOD09-C4 on day 240 shows values greater than those on day 229 on all bands. On the 7 bands, from day 229 to day 240, the respective deviations (0.011, 0.019, 0.021, 0.040, 0.059, 0.055 and 0.041) in  $R_s$ -MOD09-C5, except on band 1, were smaller than those in  $R_s$ -MOD09-C4 (0.009, 0.023, 0.035, 0.079, 0.120, 0.054 and 0.043); whereas in  $R_s$ -M2F, deviations (0.002, 0.004, 0.011, 0.009, 0.040, 0.045 and 0.023) were much smaller. With respect to deviations in  $R_s$ -MOD09-C5,  $R_s$ -M2F deviation was on average 4.8 smaller on bands 2, 3 and 4, and 1,6 lower on bands 1, 5, 6 and 7.

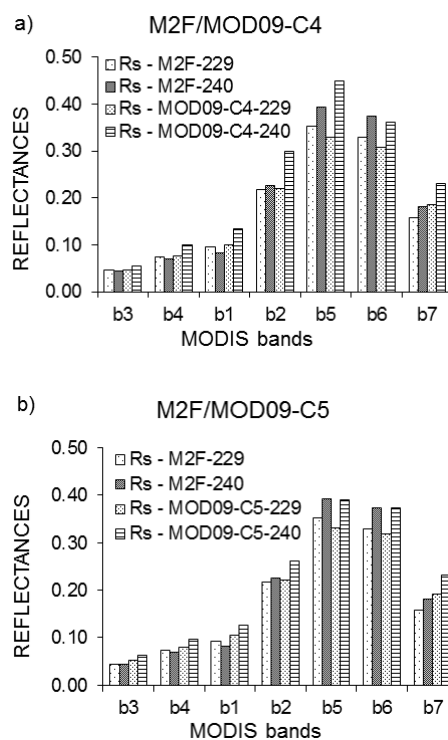


**Figure 9** – Reflectance on the seven MODIS bands on days 229 and 240 of the year 2005 in the sector illustrated in Figure 6. a) comparing reflectance  $R_s$ -M2F to  $R_s$ -MOD-C4; b) comparing reflectance  $R_s$ -M2F to  $R_s$ -MOD09-C5

The MODIS is accurate for  $\tau(0.55) < 0.3$  and smaller solar under  $45^\circ$ , however, for  $\tau(0.55) > 0.3$  and solar zenith greater than  $45^\circ$  we cannot say the same thing (Wang et al., 2010). According to Vermote & Vermeulen (1999) for  $\tau(0.55) > 0.3$  bands 1, 2 and 3, the contribution of the aerosol effects to

satellite recorded reflectance is greater than the contribution verified on the surface. Besides, bands 2, 3, 4 and 5 are those with the highest margins of error. Román et al. (2011), using a complex method for atmospheric correction, found on bands 1, 2 and 3, over an area of forest, much larger errors: 0.02; 0.04; 0.09, respectively. Liang et al. (2002), compared to the Landsat 7 ETM+, found deviations of the order of 0.015, 0.035, 0.012, 0.017, 0.039, 0.027 and 0.019 on bands 1, 2, 3, . . . , 7. It is interesting to note that the errors exposed by these authors occurred in situations with an aerosol load less than 0.5. With higher aerosol loads, as it is in our case, the error is expected to be much higher according to Verrmote & Vermeulen (1999).

Hence, under the conditions of cases 6 and 7 as shown in Table 2, the MOD09 not only presents significant errors but it does not produce reliable results after correcting the effects caused by high aerosol loads. On the other hand, the M2F provides results accurately supported in the literature (Liang et al., 2002; Schroeder et al., 2006; Tasumi et al., 2008; Liu et al., 2009; Wang et al., 2010).

#### Atmospheric correction: cases 9 and 10 (A5 sector)

In this sector, correction for days 228 and 235 in the year 2007 was done on cases 9 and 10, respectively. Data on the MCD43 were not available. Figures 10a and 10b, refer to the  $A_p$  sector on days 228  $\{\tau(0.55) = 0.64\}$  and 235  $\{\tau(0.55) = 1.37\}$ , in that order. The results from this section are relative to the subset (size:  $62 \times 64$  pixels) shown in Figure 10. It has been observed that white points on the selected area are noticed in the same position within a period of two days, so these are not clouds, these may be scars left by forest fires. In these points, the first two bits (0-1) regarding the quality of the MOD09 product are 00, ensuring that the pixels are ideal for processing the atmospheric correction on all bands. There is greater clarity on the albedo images corrected with the M2F (Figs. 10c and 10e) than on the albedo image corrected with the MOD09 (Figs. 10d and 10f). On comparisons 1, 2 and 3, we have noticed the same point found in Figures 10e and 10f in the form of a great distortion between pairs ( $A_s$ -M2F,  $A_s$ -MOD09-C5), in 1: (0.128, 0.188), 2: (0.09, 0.184) and in 3: (0.158, 0.212). Along these relationships, it has been observed that the  $A_s$ -MOD09-C5 presents in the image of day 235 points that did not appear in the image of day 228, in which the albedo is overestimated. Relation 2 is a dark pixel, whose estimated reflectance in previous sections is lower than 0.1; however, the value of  $A_s$ -MOD09 is 0.184, which may be regarded as an absurd value.

In Figure 11a, the average deviation of the  $A_s$ -M2F between columns on days 228 and 235 is 0.003. As in Figure 11, the

deviation in  $A_s$ -MOD09 is 0.017, almost 6 times higher in the M2F.

Results in this section are consistent with the results found in the previous section. Considering 0.02 as the desired accuracy for a successful atmospheric correction of satellite images (Schroeder et al., 2006), the results obtained under high aerosol load show that the M2F imparts far more reliable results than those obtained from MODIS products.

#### CONCLUSIONS

Considering the results provided, the atmospheric correction method proposed in this paper, produces reliable results in various situations.

By using the method of two streams, in order to establish the relationship between the surface reflectance and radiance at the top of the atmosphere, the adjustment made by introducing the factor  $k$  can be seen as an anisotropic effect resulting from the correction of aerosol scattering particles and air molecules on the MODIS bands 1, 2, 3 and 4, whose efficiency can be verified in the obtained results. The method, compared to other physical methods, is simple and efficient. Under conditions with higher aerosol loads, it proved more reliable than those derived from MODIS. On these, the products of collection 5 proved more efficient in relation to those from collection 4.

In case 10 (Table 2), with white blurred targets, in the albedo image derived from MODIS, collection 5, one is left with the false impression that there are clouds or even signs of burnings. This may be seen as misinformation passed on to researchers dealing with deforestation in the Amazon region. On these targets, the overestimation of albedo derived from MODIS can be derived from the adjustment of adjacent effects used on products of MODIS reflectance.

In a way, this subject needs further analysis. However, one should be careful with the correction of adjacent effects in areas with higher aerosol loads. Moreover, under conditions of lower aerosol loads, comparing the results of the  $A_s$ -M2F with those of  $A_s$ -MOD09, the correction of these effects is negligible.

Obtaining the albedo as suggested by Tasumi et al. (2008), proved effective in situations involving lower aerosol loads. Under such conditions, to obtain the reflectance for the entire solar spectrum, one should fix the corresponding weights on to each MODIS band. However, considering the aerosol load, these weights can vary significantly. This is a limitation of the method, proving it to be unresponsive to aerosol variations in the atmosphere.

In spite of the fact that the results obtained have proved satisfactory, the adjustment established between surface reflectance

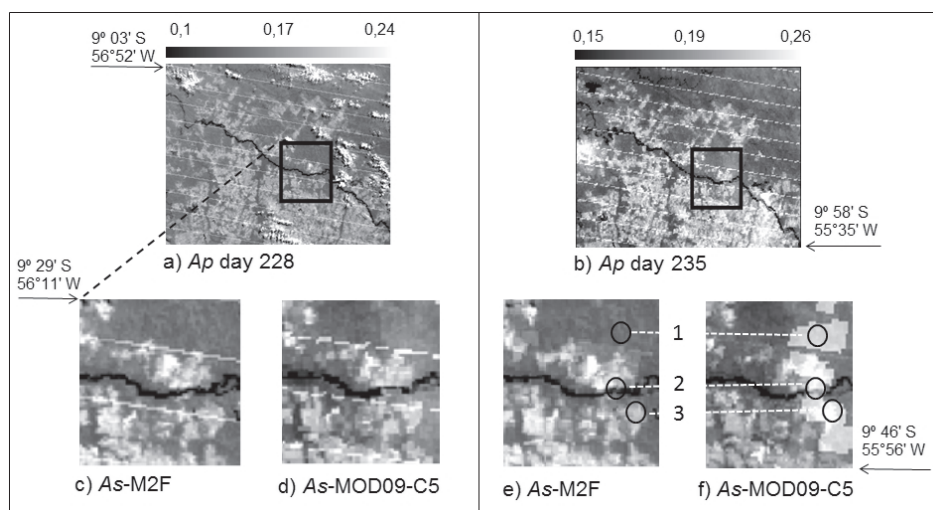


**Figure 10** – On the top, the  $A_p$  data on sector A5 on the days 228 and 235 in the year 2007; and at the bottom,  $A_p$  data relating to the subset. a)  $A_p$  for day 228, b)  $A_p$  for day 235, c)  $A_s$ -M2F from subset on day 228, d)  $A_s$ -MOD09-C5 of the subset on day 228, e)  $A_s$ -M2F of subset on day 235, and f)  $A_s$ -MOD09-C5 on day 235.

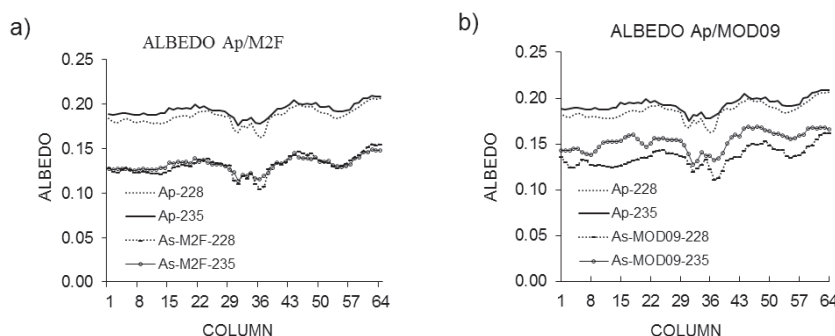


**Figure 11** – Variation of  $A_p$ ,  $A_s$ -M2F and  $A_s$ -MOD09-C5 on the subset in Figure 10 on days 228 and 235, of the year 2007 a) variation of  $A_s$ -M2F in relation to the  $A_p$ ; b) variation of  $A_s$ -MOD09-C5 with the  $A_p$ .

and radiance at the top of the atmosphere can be improved considering the geometry of incidence and viewing. For more accurate validation in areas that are not perfectly homogeneous, it is interesting take surface measurements at the various points showing differences in coverage. Similarly, by using radiometer spectrum for the errors incurred on the MODIS bands, one should correct the value of  $k$  in M2F, Eq. (6a).

**REFERENCES**

CEBALLOS JC. 1989. Stochastic properties of two-flux shortwave radiative transfer in the atmospheric. *Contrib. Atmos. Phys.*, 62: 179–192.

CHAVEZ PS Jr. 1988. An improved dark-object subtraction technique for atmospheric scattering correction of multispectral data. *Remote Sens. Environ.*, 24: 459–479.

KIDDER SQ & VONDER HAARTN. 1995. *Satellite Meteorology*, Academic Press, USA, 466 pp.

LENOBLE J. 1985. *Radiative transfer in scattering and absorbing atmospheres*. A. Deepak Publishing, 532 pp.

LIANG S, STRAHLER AH & WALTHALL C. 1999. Retrieval of Land Surface Albedo from Satellite Observations: A Simulation Study. *J. Appl. Meteorol.*, 38: 712–725.

LIANG S, FANG H & CHEN M. 2001. Atmospheric Correction of Landsat ETM+ Land, Surface Imagery – Part I: Method. *IEEE Trans. Geosci. Remote Sens.*, 39: 2490–2498.

LIANG S, FANG H, CHEN, M, SHUEY CJ, WALTHALL C, DAUGHTRY C, MORISSETTE J, SCHAAF C & STRAHLER A. 2002. Validating MODIS land surface reflectance and albedo products: Methods and preliminary results. *Remote Sens. Environ.*, 83: 149–162.

LIU J, SCHAAF C B, STRAHLER AH, JIAO Z, SHUAI Y, ZHANG Q, ROMÁN M, AUGUSTINE JA & DUTTON EG. 2009. Validation of Moderate Resolution Imaging Spectroradiometer (MODIS) albedo retrieval algorithm: Dependence of albedo on solar zenith angle. *J. Geophys. Res.*, 114: D01106.

- MEADOR WE & WEAVER WR. 1980. Two-stream approximations to radiative transfer in planetary atmospheres: A unified description of existing methods and a new improvement. *J. Atmos. Sci.*, 37: 630–643.
- MORAN MS, JACKSON RD, SLATER PN & TEILLET PM. 1992. Evaluation of simplified procedures for retrieval of land surface reflectance factors from satellite sensor output. *Remote Sens. Environ.*, 41: 169–184.
- NASA, MODIS Website. 2012. Data products. Available on: <<http://modis.gsfc.nasa.gov/data/dataproduct/>>, Access on: June 6<sup>th</sup>, 2012.
- RICCHIAZZI P, YANG S, GAUTIER C & SOWLE D. 1998. SBDART: A Research and Teaching Software Tool for Plane-Parallel Radiative Transfer in the Earth's Atmosphere. *Bull. Am. Met. Soc.*, 79: 2101–2113.
- ROMÁN MO, GATEBE CK, SCHAAF CB, POU DYAL R, ZHUOSEN WANG Z & KING MD. 2011. Variability in surface BRDF at different spatial scales (30 m–500 m) over a mixed agricultural landscape as retrieved from airborne and satellite spectral measurements. *Remote Sens. Environ.*, 115: 2184–2203.
- SCHAAF CB, GAO F, STRAHLER AH, LUCHT W, LI X, TSANG T, STRUGNELL NC, ZHANG X, JIN Y, MULLER JP, LEWIS P, BARNSLEY M, HOBSON P, DISNEY M, ROBERTS G, DUNDERDALE M, DOLL C, D'ENTREMONT RP, HUG B, LIANG S, PRIVETTE JL & ROY D. 2002. First operational BRDF albedo nadir reflectance products from MODIS. *Remote Sens. Environ.*, 83: 135–148.
- SCHROEDER TA, COHEN WB, SONG C, CANTY MJ & YANG Z. 2006. Radiometric correction of multi-temporal Landsat data for characterization of early successional forest patterns in western Oregon. *Remote Sens. Environ.*, 103: 16–26.
- SHETTLE EP & FENN RW. 1979. Models for the aerosol of the lower atmosphere and the effect of humidity variations on their optical properties. *Environ. Res.*, Paper no. 676, Air Force Geophysics Lab. Hanscom AFB, Massachusetts, EUA, 94 pp.
- SONG C, WOODCOCK CE, SETO KC, LENNEY MP & MACOMBER SA. 2001. Classification and Change Detection Using Landsat TM Data: When and How to Correct Atmospheric Effects. *Remote Sens. Environ.*, 75: 230–244.
- SOUZA JD. 2008. Modelo físico-matemático de correção atmosférica para imagens TM-Landsat 5 e MODIS-Terra/Aqua. Doctorate thesis on Meteorology, Universidade Federal de Campina Grande, 177 pp.
- SOUZA JD, SILVA BB & CEBALLOS JC. 2008. Estimativa da Radiação Solar Global a Superfície usando um Modelo Estocástico: Caso sem Nuvens. *Rev. Bras. Geog.*, 26(1): 31–44.
- TASUMI M, ALLEN RG & TREZZA R. 2008. At-surface reflectance and Albedo from Satellite for Operational Calculation of Land Surface Energy Balance. *J. Hydrol. Eng.*, p. 51–63.
- VERMOTE EF & VERMEULEN A. 1999. MODIS Atmospheric correction algorithm: spectral reflectance (MOD09). ATBD, v(4.0), NASA, contract NAS5-96062.
- VERMOTE EF, TANRÉ D, DEUZÉ JL, HERMAN M & MORCRETTE JJ. 1997. Second Simulation of the Satellite Signal in the Solar Spectrum, 6S: An Overview. *IEEE Trans. Geosci. Remote Sens.*, 35: 675–685.
- VERMOTE EF, EL SALEOUS NZ & JUSTICE CO. 2002. Atmospheric correction of MODIS data in the visible to middle infrared: first results. *Remote Sens. Environ.*, 83: 97–111.
- WANG Y, LYAPUSTIN AI, PRIVETTE JL, COOK RB, SANTHANAVANNAN SK, VERMOTE EF & SCHAAF CL. 2010. Assessment of biases in MODIS surface reflectance due to Lambertian approximation. *Remote Sens. Environ.*, 114: 2791–2801.

Recebido em 23 dezembro, 2011 / Aceito em 8 junho, 2012  
 Received on December 23, 2011 / Accepted on June 8, 2012

## NOTES ABOUT THE AUTHORS

**Juarez Dantas de Souza.** Graduated in Mathematics from the Universidade Estadual da Paraíba – UEPB (1979). PhD in Meteorology from the Federal University of Paraíba – UFPB (2008). Teaches at the UEPB where also develops research activities.

**Juan Carlos Ceballos.** Graduated in Physics from the Universidade Nacional de Tucumán, Argentina (1966). PhD in Meteorology from the Instituto Astronômico e Geofísico, Universidade de São Paulo, Brazil (1986). Research Internship on solar radiation propagation on finite clouds at the Laboratoire d'Optique Atmosphérique, Université de Lille, France. Retired Professor from the Centro de Ciências e Tecnologia, Universidade Federal da Paraíba. Researcher at the Divisão de Satélites e Sistemas Ambientais, Centro de Previsão de Tempo e Estudos Climáticos from the Instituto Nacional de Pesquisas Espaciais.

**Bernardo Barbosa da Silva.** Graduated and later obtained master degree in Meteorology. Doctorate degree in Water Resources from the Universidade Federal da Paraíba. Postdoctoral fellow from the University of Arizona. Works at the Meteorology Postgraduate Programs at the Universidade Federal de Campina Grande (UFCG), and at the Geografia e Recursos Hídricos at the Universidade Federal de Pernambuco (UFPE). Is a CNPq researcher. Has over 70 scientific papers published in both national and international journals. Has advised 35 master students and 23 doctorate students.